A Reliable Error Estimation Technique for CFD Applications

I. Celik, E. Karaismail, and D. Parsons
Mechanical and Aerospace Engineering Department
West Virginia University
Morgantown WV, 26505 (USA)

Ismail.Celik@mail.wvu.edu

ABSTRACT

Uncertainty assessment in CFD (computational fluid dynamics) ultimately relies on the estimation of the true discretization error defined as the difference between the exact (unknown) solution to the partial differential equation and the numerical solution obtained from a discretized equation on a certain grid represented by the computational cell size, h. The commonly used Richardson extrapolation to zero-grid size to determine the extrapolated exact solution has limited success and requires intensive calculations on at least three and sometimes up to 5 or 6 grids. Even then questions related to oscillatory convergence or divergence, the anomalies concerning the observed (or apparent) order of the computations can not be resolved. The technique proposed in this study attempts to avoid much of the difficulties of Richardson extrapolation by focusing on reliable estimators for the local true error. The technique is based on the refinement of ideas presented by Celik and Li [1] concerning the relation between the approximate error and the true error. The relations used in the present study are derived using theoretical considerations. The proposed method is verified using manufactured solutions for 1D and 2D scalar transport, for boundary layer type flows as well as for flows representative of the commonly used backward-facing step bench-mark. If the reliability of this technique can be demonstrated for more complex problems it will open many opportunities beyond uncertainty estimation such as adaptive grid refinement.

1.0 INTRODUCTION

Along with the exponential increase in applications of CFD the interest in formulating some kind of quality control on the CFD solutions has increased. Starting with ASME (American Society of Mechanical Engineers), many professional organizations have followed suit and implemented policies for 'statement of uncertainty' in CFD results. The uncertainty measures are usually based on some error estimates. The errors are primarily related to iteration convergence, grid convergence, and modeling errors among many others. This paper focuses on grid-convergence error also referred to as discretization errors. The iteration errors can be significant [2, 3, 4, 5] however, in this work we reduce them to very small values so that they do not pollute the solution, hence the dominant numerical error is associated with discretization.

The recommended method for discretization error estimation is the RE (Richardson extrapolation) method. Since its first elegant application by its originator Richardson [6, 7], this method has been studied by many authors. Its intricacies, shortcomings and generalization have been widely investigated. A short list of references given in the bibliography [8, 9, 10, 11, 12, 13, 14, 15, 16, 17] is selected for the direct relevance of these references to the subject, and for brevity. But, the RE method is far from perfect. The local RE values of

Celik, I.; Karaismail, E.; Parsons, D. (2007) A Reliable Error Estimation Technique for CFD Applications. In *Computational Uncertainty in Military Vehicle Design* (pp. 32-1 – 32-20). Meeting Proceedings RTO-MP-AVT-147, Paper 32. Neuilly-sur-Seine, France: RTO. Available from: http://www.rto.nato.int.

the predicted variables may not exhibit a smooth, monotonic dependence on grid resolution, and in a time-dependent calculations, this non-smooth response becomes a function of time and space. Nonetheless, it is currently the most robust method available for the prediction of numerical uncertainty. The method presented here can be considered as a variant of RE with more desirable features.

Since there are many ways for estimating numerical uncertainty and errors, which are based on certain assumptions, such as monotonic convergence, and being in the asymptotic range in case of RE, it is imperative that these methods be also validated using some benchmarks. This need has clearly become apparent during the First Workshop on CFD Uncertainty Analysis in Lisbon [18]. These benchmarks should be analytical solutions that resemble those of Navier-Stokes equations for a class of flow problems. In the 2nd Lisbon Workshop [19] a boundary-layer type of analytical solution was used to test various error and uncertainty estimators. Most methods performed well for this relatively simple grid on relatively fine meshes. The question remained that what would be the outcome for a relatively more complex problems such as the separated flow over a backward facing step on relatively coarse grids.

It is this question that we attempt to answer in this current work. To do this we needed an analytical solution that resembled the well known flow over backward facing step. This is developed first, then a commercial software is used to obtain the solution on various set of grids and the error estimators are applied to the results with the aim of estimating the discretization error. The results from the case with a boundary-layer type flow are also presented for comparison.

2.0 ERROR ESTIMATION METHODS

The method developed to predict the true error is a variant of the extrapolation method proposed by Celik *et al*. [1, 20] named Approximate Error Spline method (AES). This method assumes that the true error, E_t is proportional to the approximate error, E_a, as shown by the following equation

$$E_t^h = cE_a^h \tag{1}$$

where the true error is defined by

$$E_t^{\ h} = \phi - \phi_h \tag{2}$$

and the approximate error given as

$$E_a^{\ h} = \phi_h - \phi_{\alpha h} \tag{3}$$

In Eqs. (2 and 3) α is the grid refinement or coarsening factor i.e. $\alpha_1=h_2/h_1$, $\alpha_2=h_3/h_2$, etc., where h_i represents the average grid size, also $h_1 < h_2 < h_3$ which means that subscript "1" denotes the smallest grid size (fine grid) and subscript "3" the coarsest grid.

In order to apply Eq. (1) three grid calculations (triplet) are needed. The post-processing of the numerical calculations and making use of Eq. (1) enables determination of the proportionality constant c. This global constant c is calculated from the local constants as follows

$$c = \frac{1}{2}\frac{\left\|c_{i,j}^1\right\|_\infty + \left\|c_{i,j}^2\right\|_\infty}{N} \tag{4}$$

where N is the total number of grid points and

$$c_{i,j}^{1} = \frac{\phi_2^{i,j} - \phi_1^{i,j}}{\phi_3^{i,j} - 2\phi_2^{i,j} + \phi_1^{i,j}} \tag{5a}$$

$$c_{i,j}^{2} = \frac{\phi_3^{i,j} - \phi_2^{i,j}}{\phi_3^{i,j} - 2\phi_2^{i,j} + \phi_1^{i,j}} \tag{5b}$$

Note that Eqs. (5a) and (5b) represent the proportionality constant using the finest triplet (1, 2, 3) but the method is not limited to the use of that triplet, however the use of the finest triplet is expected to give a more accurate estimation of the true error.

3.0 DESIGN OF APPROXIMATE SOLUTIONS

3.1 Case-3: Boundary-layer type flow:

We employ the method of manufactured solutions proposed by Roache [22] to obtain approximate solutions to Navier-Stokes equations. The solution to Case-3 (Boundary-layer type flow), was derived with the help of D. Pelletier (private communication) and published in [19], hence details will not be repeated here. The analytical expressions used for the velocity components, and pressure are as follows:

The x-velocity component is given by

$$u = erf(\eta) \tag{6}$$

where the dimensionless variable η is given by

$$\eta = \frac{\sigma y}{x};\ \sigma = 4.0 \tag{7}$$

The y- velocity component is given as follows

$$\upsilon = \frac{1}{\sigma\sqrt{\pi}}\left(1 - e^{-\eta^2}\right) \tag{8}$$

while the pressure field is

$$C_p = \frac{P}{\rho U_{ref}^{\ 2}} = 0.5\ln\left(2x - x^2 + 0.25\right)\ln\left(4y^3 - 3y^2 + 1.25\right) \tag{9}$$

Equations (6) to (9) represent dimensionless quantities but all the reference quantities were selected as unity. Therefore the dimensionless and dimensional quantities are equivalent.

3.2 Case-4: Separated flow

For the case of separated flows (Case-4), we work with a two-dimensional stream function so that the derived velocity components automatically satisfy continuity. The stream function, ψ, is decomposed in to two parts, one satisfying the boundary conditions, ψ_b, and the other is a solution that does not contribute to flow rate and satisfies homogeneous boundary conditions, namely, ψ_s

$$\psi = \psi_b + \psi_s \tag{10}$$

We let

$$\psi_b = f_b g_b + (1 - g_b) h_b \tag{11}$$

Such that f_b and h_b are functions of $\eta = \frac{y}{H}$ where H is the channel height, and g_b is only a function of $\varepsilon = \frac{x}{L}$ where L is the channel length; f_b and g_b satisfying the following conditions

$$\begin{gathered} f_b(0) = f_b'(0) = 0, \quad f_b(1) = 1, \quad f_b'(1) = 0 \\ g_b(0) = 1, \quad g_b'(0) = 0, \quad g_b(1) = 0 \end{gathered} \tag{12}$$

Therefore f_b' represents the axial velocity at the inlet and h_b' represents the axial velocity profile at the outlet. Thus no-slip velocity condition at the walls, i.e, $\eta = 0$ and $\eta = 1$ are also satisfied.
Then we select

$$f_b(\eta) = \sin^2\left(\frac{\pi}{2}\eta\right) e^{-\alpha(1-\eta)^2} \tag{13}$$

Where $\alpha = \frac{\alpha^*}{(1-\eta_s)^2}$ and α^* is a constant and set to 9.0.

and

$$h_b(\eta) = \sin^2\left(\frac{\pi}{2}\eta\right) \tag{14}$$

$$g_b(\varepsilon) = \cos^2\left(\frac{\pi}{2}\varepsilon\right) \tag{15}$$

And further we let

$$\psi_s = f_s g_s \tag{16}$$

where the functions f_s and g_s are given below

$$f_s(\eta, \varepsilon) = A\left[\eta - h_s(\varepsilon)\right]\eta^2 (1-\eta)^2 \tag{17}$$

where A=10 and $h_s(\varepsilon)$ is given as

$$h_s(\varepsilon) = \begin{cases} \eta_{step} \dfrac{1 + \cos\left(\pi \dfrac{\varepsilon}{\varepsilon_r}\right)}{2} & (\varepsilon \le \varepsilon_r) \\ 0 & (\varepsilon > \varepsilon_r) \end{cases} \tag{18}$$

and ε_r is the dimensionless reattachment length of the flow.

$$g_s(\varepsilon) = B\varepsilon^2(1-\varepsilon)^2 e^{-\beta\varepsilon^2} \tag{19}$$

where $\beta = \dfrac{\beta^*}{\varepsilon_r^{\,2}}$. β^* and B are constants and set to 5.0 and 100, respectively.

The corresponding velocity components are given by

$$u = \frac{\partial \psi}{\partial y} \quad \text{and} \quad v = -\frac{\partial \psi}{\partial x} \tag{20}$$

The corresponding source gradients are determined from the Navier Stokes equation using the above expressions for the axial (u) and stream-wise (v) velocities. These velocities can be found in Appendix A more explicitly. These sources may or may not represent pressure gradient terms. They will correspond to a pressure field only if the vorticity transport equation is satisfied, otherwise these terms may be interpreted as contributions from other phenomena such as turbulence modeling.

4.0 APPLICATION

4.1 Case-1: One-Dimensional Scalar Transport Equation

The one dimensional steady scalar transport equation given by

$$Pe_L \phi_x = \phi_{xx} + S_\phi \tag{21}$$

has the following analytical solution

$$\phi = \frac{\exp(Pe_L \varepsilon) - \exp(Pe_L)}{1 - \exp(Pe_L)} \tag{22}$$

where the Peclet number is defined as $Pe_L = \bar{u}L/\Gamma$. Nondimensional length, ε is taken as $\varepsilon = x/L$, L being the total length of the domain.

The grids (triplet) used to solve numerically the 1-D scalar transport equation consisted of 11, 21 and 41 nodes. These grids are referred from now on as coarse, medium and fine grid respectively. The analytical solution along with the numerical solution on the three grids is shown in Fig. 1. As can be seen from the figure, numerical solution approaches to the analytical solution as the grid is refined (i.e. fine grid). Fig. 2 illustrates a comparison of true, approximate, and estimated error calculated on different grids and by different methods.

The equations used to calculate the true error and approximate error on the medium grid are given by

$$E_t^{fm} = \phi_{fm}^{ana} - \phi_m^{num}; \qquad E_a^{fm} = \phi_{fm}^{num} - \phi_m^{num} \tag{23a}$$

where the subscripts and/or superscripts *f, m, c* mean fine, medium and coarse grid. When the subscripts/superscripts shown above appear together it means that the first grid (on the left) was interpolated

to the second grid (on the right). The superscripts *ana* and *num* denote analytical and numerical solutions respectively. Also the subscripts *a* and *t* denote approximate and true respectively. Similarly the true and approximate error on the coarse grid are calculated by

$$E_t^{mc} = \phi_{mc}^{ana} - \phi_c^{num}; \qquad E_a^{mc} = \phi_{mc}^{num} - \phi_c^{num} \tag{23b}$$

One of the two estimated errors presented in Fig. 2 is based on the local value of the proportionality constant as described by Eq. (5), and the other one is calculated using a uniform proportionality constant over the whole domain whose value calculated with Eq. (4) is 1.37 in this case. The reasoning of the latter case is that the true error is proportional to the approximate error, then for engineering calculations it would be advantageous to use such a global proportionality constant which in fact bounds the true error while the local constant does not. Another advantage would be that the calculation of the local proportionality constant in real engineering cases (e.g. three dimensional complex flow problems) would be complicated and expensive from the computational point of view.

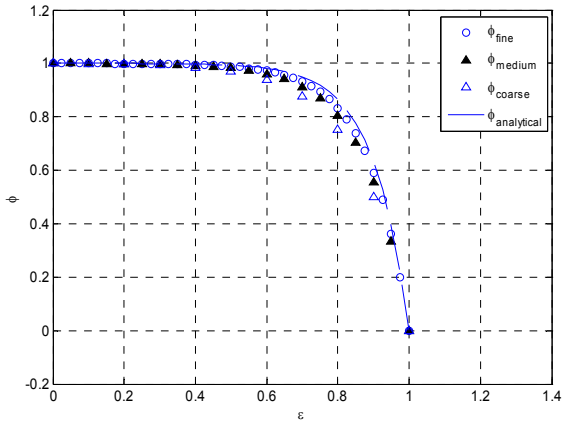

Figure 1: Analytical and numerical scalar solutions on three different grids

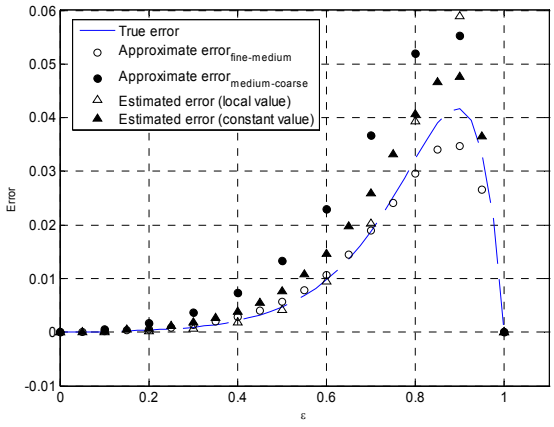

Figure 2: True error, approximate error and estimated error on the solution of the scalar

4.2 Case-2: Two-Dimensional Scalar Transport Equation

A generic scalar field, in two dimensions, is solved using the fixed flux approach in Fluent. Here the velocity field is prescribed, and the analytical solution is forced using the method of manufactured solution. Dirichlet boundary conditions were prescribed for the solution of this equation. For the case of incompressible, two-dimensional flow the velocity field is given by the following analytic functions such that they satisfy the equation of continuity.

$$u = \left(\frac{H}{H_{\exp and}}\right) y^*\left(2 - y^*\right) - \sin\left(2\pi y^*\right) x^*\left(1 - x^*\right) \tag{24}$$

$$v = \left(-\frac{1}{2\pi}\right)\left[\cos\left(2\pi y^*\right) - 1\right]\left(1 - 2x^*\right)\left(\frac{H_{\exp and}}{L}\right) \tag{25}$$

In Eq. (24) and Eq. (25) non-dimensional coordinates x^* and y^* are defined by

$$x^* = \frac{x - x_{step}}{L} \; ; y^* = \frac{y}{H_{\exp and}} \tag{26}$$

The scalar field is given by the following expression composed of functions of x and y

$$\phi = f(x) f(y) + C_1 f(y) g(x) \tag{27}$$

where the functions in Eq. (27) are defined below

$$f(x) = \cos(w_x)\cos(w_x) \;\; ; \; w_x = w_{freq} x^* \;\; ; \;\; w_{freq} = 0.5\pi \tag{28a}$$

$$f(y) = y^{*2}\left(1 - y^*\right)^2 \tag{28b}$$

$$g(x) = x^{*2}\left(1 - x^{*2}\right) \tag{28c}$$

Finally the source term for the scalar transport equation can be determined using Eqs. (24) to (28) and their derivatives

$$Source = u\phi_x + v\phi_y - C_{UDSI}(\phi_{xx} + \phi_{yy}) \tag{29}$$

Where C_{UDSI} denotes the user defined transport (diffusivity/conductivity) coefficient.

The set of three grids used to solve the two-dimensional scalar transport equation numerically is $20 \times 20,\ 40 \times 40,$ and 80×80. In Fig. 3 and 4 the true error and approximate error is presented.

Fig. 3 represents the case when the scalar transport equation is dominated by convection. As can be seen the proportionality constant between the true error on the medium grid and the approximate error between fine and medium grid is close to 2.5 (Figs. 3(a) and 3(b)); this constant between the true error on the coarse grid and the approximate error between medium and coarse grid is around 2.25. The proportionality constant calculated from Eq. (4) is 2.52 for the case mentioned above and shown in Fig. 3. Therefore it can be said that the true error can be estimated and bounded using the proportionality constant reported above along with the approximate error. Similarly in the diffusion dominated case (Fig. 4) the true error can be bounded by the approximate error when the proportionally constant is calculated with Eq. (4) resulting in a value of 1.6. It is important to note that the methodology described for the estimation of the true error also bounds the interpolation error.

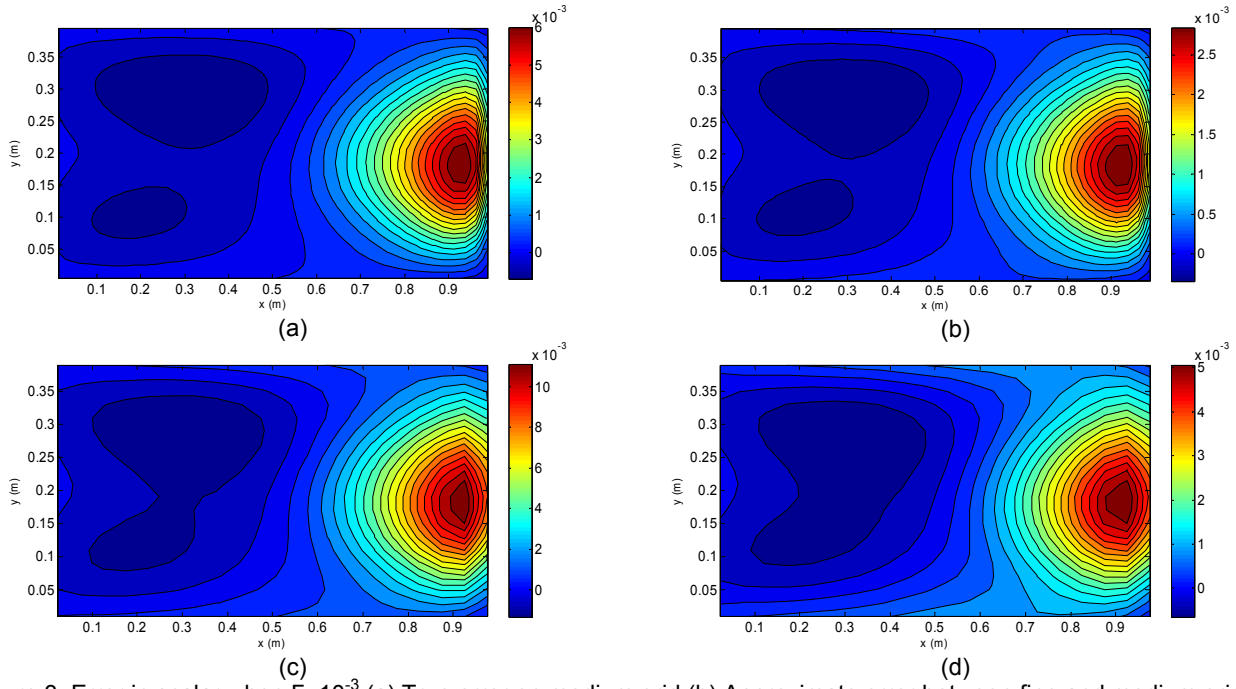

Figure 3: Error in scalar when $\Gamma=10^{-3}$ (a) True error on medium grid (b) Approximate error between fine and medium grid (c) True error coarse grid (d) Approximate error between medium and coarse grid

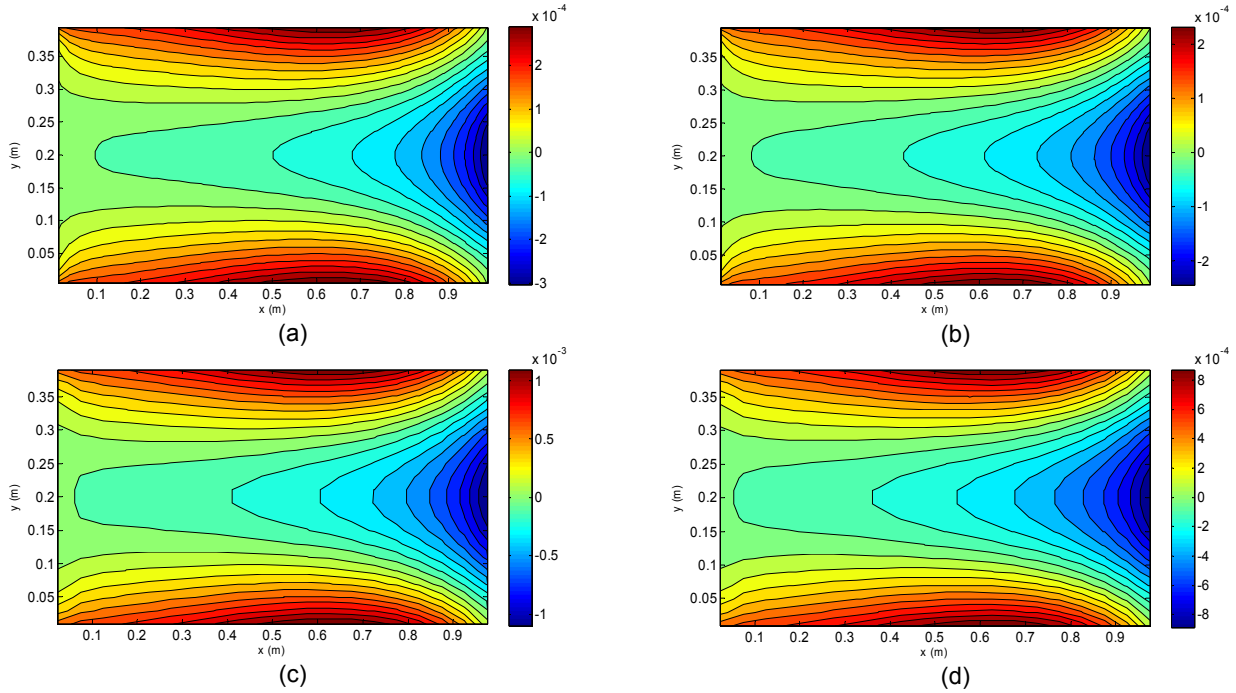

Figure 4: Error in scalar when $\Gamma=10$ (a) True error on medium grid (b) Approximate error between fine and medium grid (c) True error coarse grid (d) Approximate error between medium and coarse grid

4.3 Case-3: Boundary-layer type flow

The computational domain for the manufactured solution is a square with the following dimensions: $0.5 \leq x \leq 1$ and $0 \leq y \leq 0.5$. Except for the south (bottom) boundary, the boundary conditions prescribed were the analytical velocity profiles expressed in terms of x and y components. The south boundary was set as a wall with the no-slip condition. In order to predict the true error as shown in Section 2 several cases were run. The studied cases differ from each other in their grid density. An orderly grid refinement was done between each case. Between cases the average grid size was decreased by a factor of four.

The selected grids were structured, non-uniform with an expansion ratio of 0.95 in y-direction. The grid in y-direction is finer near the south boundary in order to predict, with reasonable accuracy, the velocity gradients inside the wall boundary layer. Along the x-direction the grid is uniform.

In Fig. 5 the true error and the estimated true error for x-velocity component are shown. Similarly in Figs. 6 and 7 the error contours for y-velocity component and pressure are presented respectively. The results shown in this section are based on the triplet (three grid calculations) 15×15, 30×30 and 60×60. The discretization scheme of the convective term is 1st order upwind. As can be seen in Figs. 5, 6 and 7 the estimated true errors match qualitatively and quantitatively the true error. The calculated global proportionality constants for u velocity, v velocity and pressure given by Eq. (4) are 1.87, 1.58 and 1.26 respectively. With the proportionality constants mentioned above the estimated true error nearly bounds the true error.

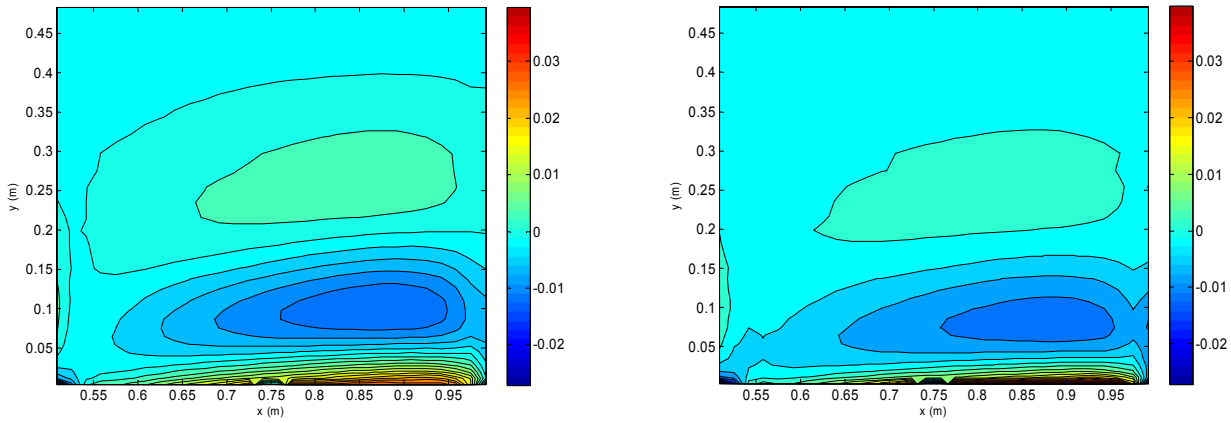

(a) (b)

Figure 5: Error contours for x-velocity component; (a) True error on medium grid, (b) Estimated true error

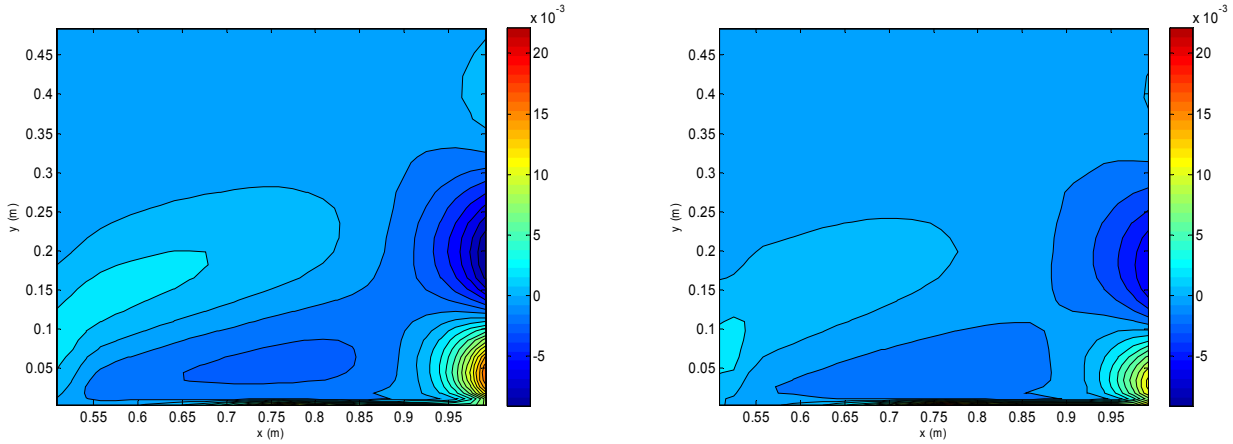

(a) (b)

Figure 6 Error contours for y-velocity component; (a) True error on medium grid, (b) Estimated true error

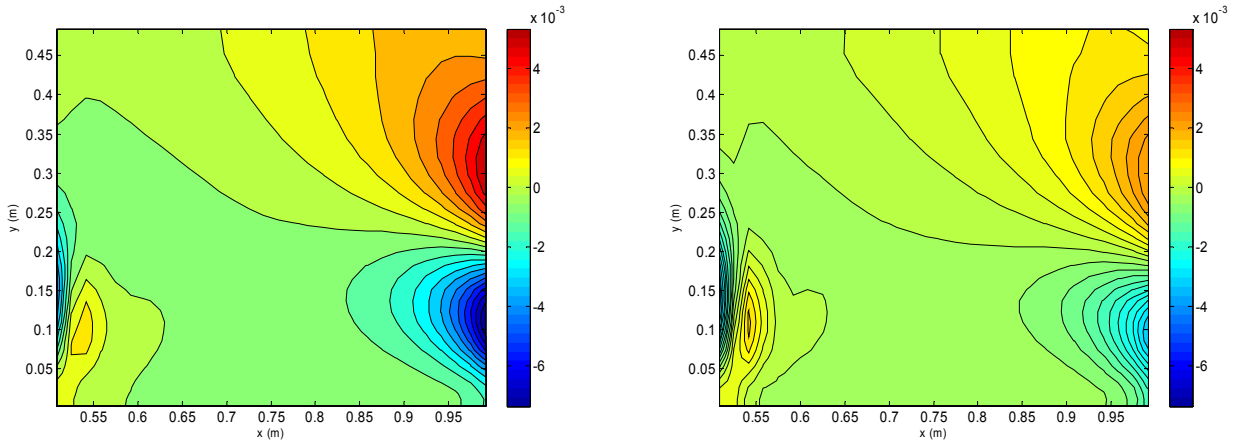

(a) (b)

Figure 7 Error contours for pressure; (a) True error on medium grid, (b) Estimated true error

4.4 Case-4: Separated flows (Backward Facing Step)

Having validated the error estimation technique on aforementioned cases, we applied it to a relatively complicated case of flow over a backward-facing step. The physical system under consideration consists of a flow past a backward-facing step with expansion ratio 5/4. The step is located at the inlet ($x = 0$) in order to simplify geometry and hence the analytical solution. The length, L of the domain is 10 step heights, h_{steps}.

For an effective Reynolds number $\left(\mathrm{Re}_{eff} = u_{avg} h_{step} \big/ \upsilon_{eff}^{avg}\right)$ of 10, based on the step height (h_{step}=1.0m), and average velocity at the inlet (u_{avr} = 0.25m/s), analytical solutions for the axial and vertical velocities were obtained by employing Eqs. (10)-(20). These equations had been designed by taking the boundary conditions into account. The imposed boundary conditions are

$$u_{in} = \left.\frac{\partial \psi}{\partial y}\right|_{x=0} \qquad u_{out} = \left.\frac{\partial \psi}{\partial y}\right|_{x=L} \quad \text{and} \quad u_{wall} = 0 \quad \text{(no slip)} \tag{30}$$

$$v_{in} = -\left.\frac{\partial \psi}{\partial x}\right|_{x=0} \qquad v_{out} = -\left.\frac{\partial \psi}{\partial x}\right|_{x=L} \quad \text{and} \quad v_{wall} = 0 \quad \text{(no slip)} \tag{31}$$

The governing transport equations were modified by implementing source terms (S_x, S_y) obtained from the analytical solution so that the errors induced by different interactions occurring in the flow were damped. Derivation of these source terms can be found in Appendix B. Consequently, the x- and y-components of modified momentum equation take the following forms, respectively.

$$u\frac{\partial u}{\partial x} + v\frac{\partial u}{\partial y} = -\frac{1}{\rho}\frac{\partial p}{\partial x} + \upsilon_{eff}^{avg}\left[\frac{\partial^2 u}{\partial x^2} + \frac{\partial^2 u}{\partial y^2}\right] + S_x \tag{32}$$

$$u\frac{\partial v}{\partial x} + v\frac{\partial v}{\partial y} = -\frac{1}{\rho}\frac{\partial p}{\partial y} + \upsilon_{eff}^{avg}\left[\frac{\partial^2 v}{\partial x^2} + \frac{\partial^2 v}{\partial y^2}\right] + S_y \tag{33}$$

The source terms in the above equations are evaluated from analytical expressions obtained as the remainder of x-momentum and y-momentum equations when the analytical expressions for the velocity components are substituted for the convection and diffusion terms. The density appearing in these equations was taken as unity.

These equations, subject to the same analytic boundary conditions, were solved together with the continuity equation using the commercial CFD package FLUENT 6.3.

At this juncture, it should be noted that for the outlet boundary imposing the velocity boundary condition obtained from the analytical solution is crucial because the use of pressure outlet or outflow boundary conditions results in incorrect velocity profiles. Comparisons of these velocity profiles are illustrated in Fig. 8.

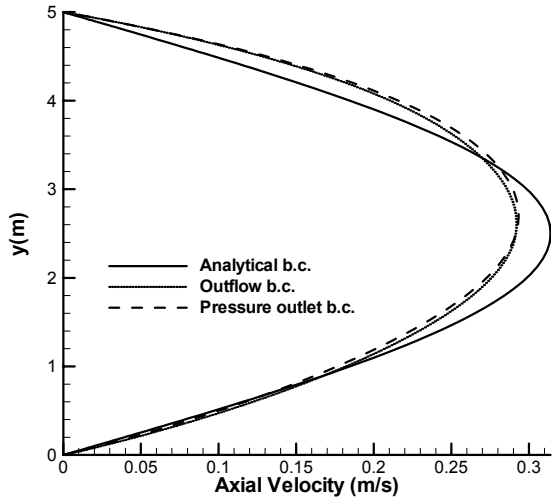

Figure 8: Axial velocity profiles at the outlet for different boundary conditions

The convective and diffusive terms in the momentum equations were discretized with first order upwind and central difference schemes, respectively. Double precision is used for all the calculations so that the round-off errors are minimized. The executions were terminated when the scaled residual for the continuity equation approached an asymptotic value.

The numerical error in the calculations was assessed by repeating the numerical computations on a set of three grids with different resolutions. For the purpose of the study an orderly grid refinement was carried out by doubling the coarser grid. On the whole, nonuniform grids (clustered to the upper and lower walls) with resolutions of 200×100, 400×200 and 800×400 in x and y directions, respectively, were employed in this study.

Once the analytical and numerical solutions are obtained for the same conditions, a comparison can be made to test their proximity. Figs. 9 and 10 show the velocity fields obtained from analytical and numerical solutions on the fine grid, respectively.

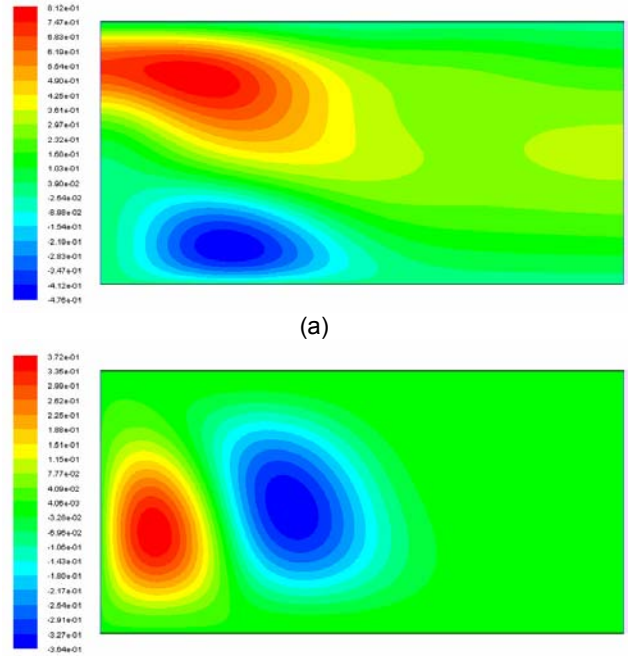

(a)

(b)

Figure 9: Velocity field from analytical solution
(a) Axial velocity, (b) Vertical velocity

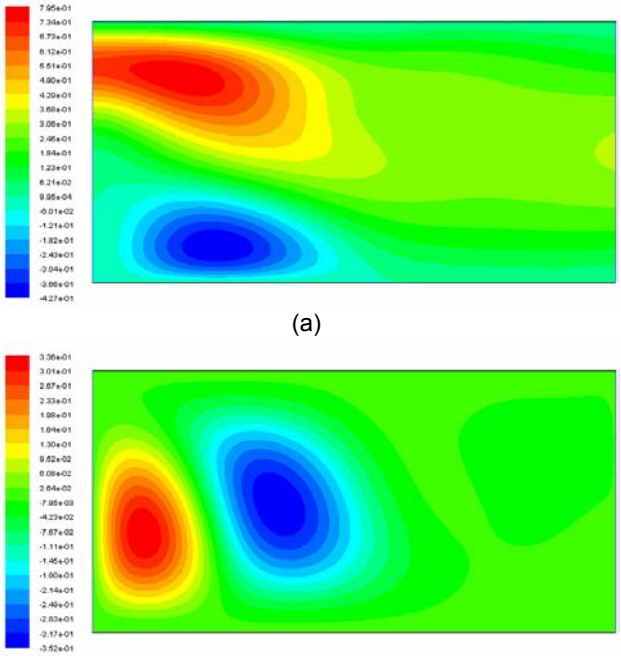

(a)

(b)

Figure 10: Velocity field from numerical solution on the (800x400) grid
(a) Axial velocity, (b) Vertical velocity

The excellent agreement between the fine grid solution and the analytical solution is a strong indication of the quality of the analytical solution and it shows that as the grid is refined the numerical solution approached the exact solution satisfying the consistency condition for the numerical scheme used. This is also an indication that the analytical solution can be confidently used as an exact solution for error estimation purposes.

In a way similar to the boundary layer flow, the true errors and approximate errors in the axial and vertical velocity distributions were calculated and depicted in Figs. 11 and 12, respectively. Although there is good qualitative agreement between the true error and the approximate error distribution, a closer look reveals that

the location of the maxima and minima of the two do not correspond closely. The reasons for these are being investigated.

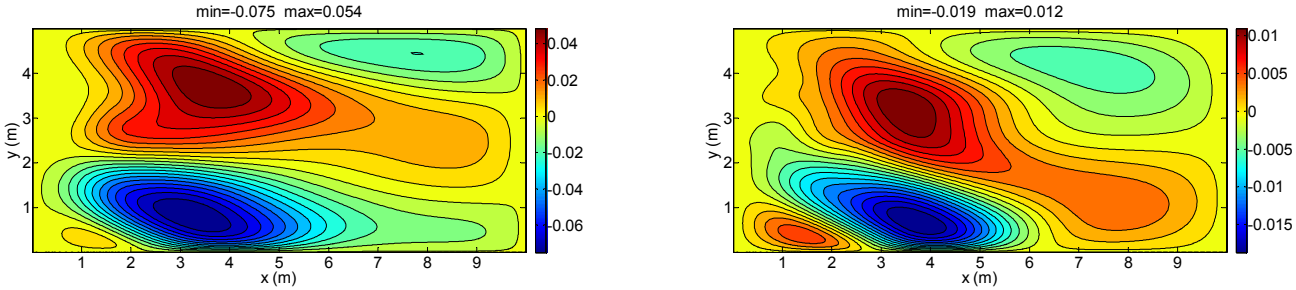

Figure 11: Error in axial velocity (a) True error on medium grid, (b) Approximate error between fine and medium grid

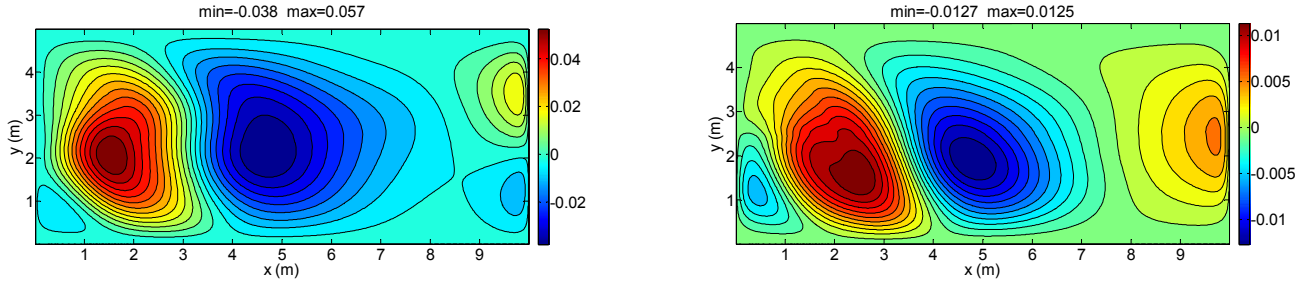

Figure 12: Error in vertical velocity (a) True error on medium grid, (b) Approximate error between fine and medium grid

On the other hand, the average proportionality constants for the axial velocity are c_1 = 2.12 and c_2= 2.30 and for the vertical velocity c_1 = 2.67 and c_2=3.55 with the corresponding averages of 2.21 and 3.11. When these factors are used the approximate errors still underestimate the true errors in magnitude, but the trends are similar. A quantitative comparison can be seen in Figs. 12 and 13 where the estimated error and true error are compared at selected locations. Here only the magnitudes are compared since the sign of the error may not be important in most applications. It is seen again that the trends are very similar but the magnitudes of true error is underestimated using the current method. In view of these observations, it can be concluded that in order to make a reliable statement on this case further investigation is needed.

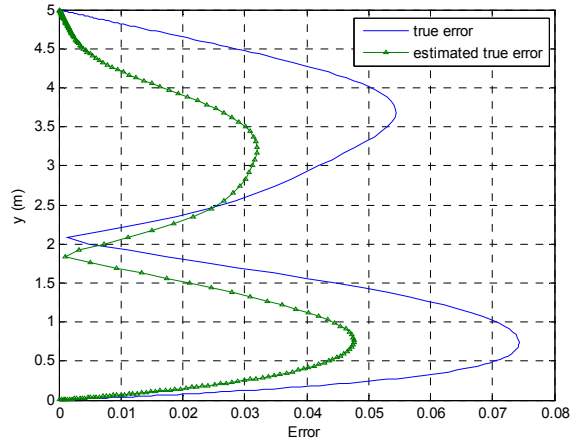

(a)

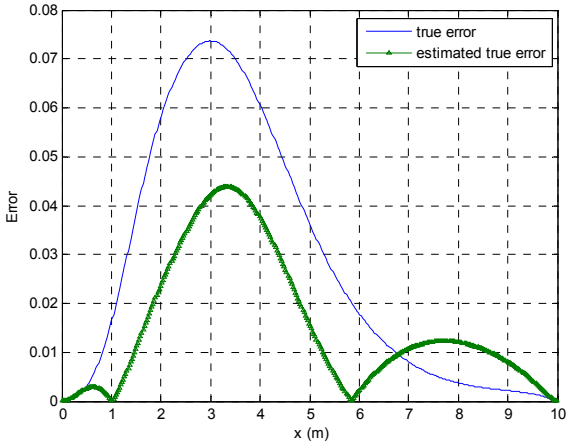

(b)

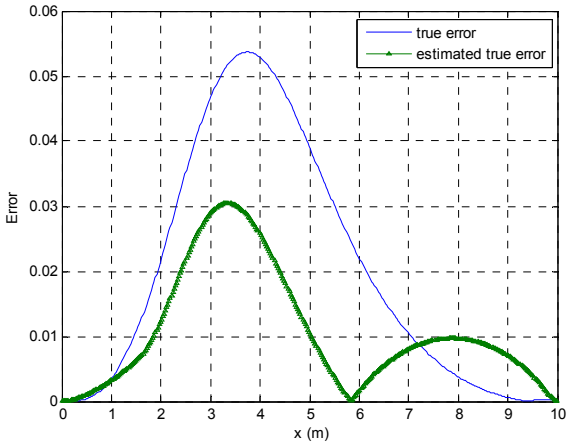

(c)

Figure 12: Estimated true error in axial velocity at (a) x= 3.5m, (b) y=1m, (c) y=3.5m

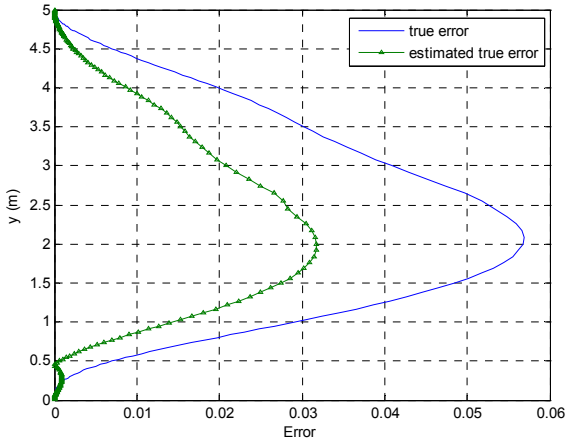

(a)

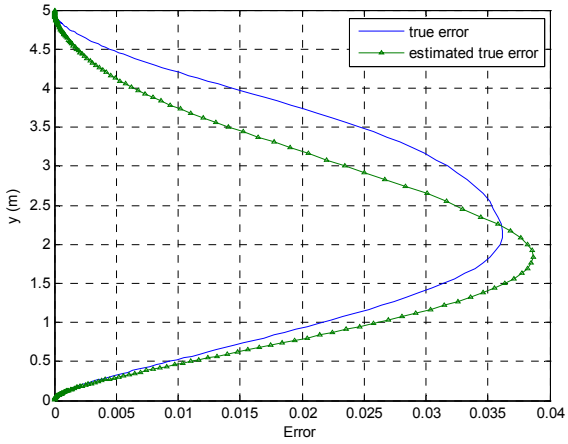

(b)

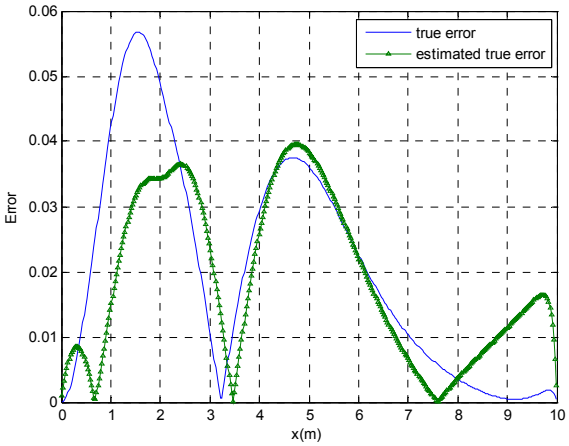

(c)

Figure13: Estimated true error in vertical velocity at (a) x= 1.5m, (b) x=5m, (c) y=2m

5.0 CONCLUSIONS AND RECOMMENDATIONS

A fairly simple error estimation method based on the original idea of Richardson extrapolation is proposed. This method assumes that, at least, in the asymptotic range the approximate error, i.e. the difference between consecutive solutions on similar grids, is proportional to the true error, i.e. the difference between the exact (usually unknown) solution and the numerical solution. The proportionality coefficient is calculated as an average value of the local coefficients calculated using a set of three numerical solutions on three different grids. The method is verified on 1D and 2D scalar transport, and applied to 2D Navier-Stokes equations for a parabolic type flow and also for a separated flow resembling that of flow over backward facing step. All indications are that this method gives reliable estimates of the error even on relatively coarse grids. The calculated constant of proportionality seems to be low for the cased involving Navier -stokes solutions. The reasons for this are currently being investigated. A temporary fix would be to use $\max(c_1, c_2)$ for conservative, and the average for nonconservative purposes. Another advantage of this method is interpolation errors that scale with the grid size can be automatically taken into account.

6.0 ACKNOWLEDGMENTS

Significant contribution by Francisco Elizalde-Blancas is acknowledged with appreciation. The authors also thank Francisco A. Pino-Romainville for his help in Case 2.

7.0 REFERENCES

[1] Celik I, Li J. Assessment of numerical uncertainty for the calculations of turbulent flow over a backward-facing step. *International Journal for Numerical Methods in Fluids* 2005; **49**:1015–1031.

[2] Eça, L. and Hoekstra, M. “On the Influence of the Iterative Error in the Numerical Uncertainty of Ship Viscous Flow Calculations,” *26th Symposium on Naval Hydrodynamics*, Rome, Italy, 17-22 September, 2006.

[3] Ferziger, J.H., 1989 “Estimation and Reduction of Numerical Error,” *ASME Winter Annual Meeting*, San Fransisco, December, 1989

[4] Ferziger, J.H., Peric, M. (1996) “Further Discussion of Numerical Errors in CFD,” *International Journal for Numerical Methods in Fluids*, 1989; 23: 1263-1274.

[5] Stern, F., Wilson, R., and Shao, J. (2006) “Quantitative V&V of CFD Simulations and Certification of CFD Codes.” *Int. Journal of Numer. Meth. Fluids*, Vol. 50, pp. 1335-1355

[6] Richardson, L.F. (1910) “The Approximate Arithmetical Solution by Finite Differences of Physical Problems Involving Differential Equations, with an Application to the Stresses In a Masonary Dam,” *Transactions of the Royal Society of London*, Ser. A, Vol. 210, pp. 307-357.

[7] Richardson L.F. and Gaunt, J. A. (1927) “The Deferred Approach to the Limit,” *Philos. Trans. R. Soc. London Ser. A*, Vol. 226, pp. 299-361.

[8] Celik, I., Chen, C.J., Roache, P.J. and Scheurer, G. Editors. (1993), “Quantification of Uncertainty in Computational Fluid Dynamics,” ASME Publ. No. FED-Vol. 158, *ASME Fluids Engineering Division Summer Meeting*, Washington, DC, 20-24 June.

[9] Celik, I., Karatekin, O. (1997), "Numerical Experiments on Application of Richardson Extrapolation With Nonuniform Grids," *ASME Journal of Fluid Engineering*, Vol. 119, pp.584-590.

[10] Eca, L. and Hoekstra, M. (2002), "An Evaluation of Verification Procedures for CFD Applications," *24th Symposium on Naval Hydrodynamics*, Fukuoka, Japan, 8-13 July.

[11] Freitas, C.J. (1993), "Journal of Fluids Engineering Editorial Policy Statement on the Control of Numerical Accuracy," *Journal of Fluids Engineering*, Vol. 115, pp. 339-340.

[12] Roache, P.J., (1993) "A Method for Uniform Reporting of Grid Refinement Studies," Proc. Of Quantification of Uncertainty in Computation Fluid dynamics, Edited by Celik, et al., *ASME Fluids Engineering Division Spring Meeting*, Washington D.C., June 230-240, ASME Publ. No. FED-Vol. 158.

[13] Roache, P. J. (1998), "Verification and Validation in Computational Science and Engineering, " Hermosa Publishers, Albuquerque.

[14] Stern, F., Wilson, R. V., Coleman, H. W., and Paterson, E. G. (2001), "Comprehensive Approach to Verification and Validation of CFD Simulations - Part 1: Methodology and Procedures," *ASME Journal of Fluids Engineering*, Vol. 123, pp. 793-802, December.

[15] Broadhead, B.L., Rearden, B.T., Hopper, C.M., Wagschal J.J., Parks,C.V., (2004), "Sensitivity- and Uncertainty-Based Criticality Safety Validation Techniques," *Nuclear Science and Engineering*, Vol. 146, pp. 340–366.

[16] DeVolder, B., Glimm, J., Grove, J. W., Kang, Y., Lee, Y., Pao, K., Sharp, D. H., Ye, K., (2002), "Uncertainty Quantification for Multiscale Simulations," *Journal of Fluids Engineering*, Vol. 124, Issue 1, pp. 29-41

[17] Oberkampf, W.L., Trucano, T.G., and Hirsch , C., (2003), "Verification, validation, and predictive capability in computational engineering and physics," Sandia Report SAND2003-3769.

[18] Eca L, Hoekstra M (eds). *Proceedings of the Workshop on CFD Uncertainty Analysis*, Lisbon, 21-22 October, 2004

[19] Eca L, Hoekstra M (eds). *Proceedings of the 2nd Workshop on CFD Uncertainty Analysis*, Lisbon, 19-20 October, 2006

[20] Celik I, Li J, Hu G, Shaffer C. Limitations of Richardson extrapolation and some possible remedies. *ASME Journal of Fluids Engineering* 2005; 127:795 –805.

[21] Roache, P. I. "Perspective: a method for uniform reporting of grid refinement studies". *ASME Journal of Fluids Engineering* 1994; 116; 405-413.

[22] Roache, P. J. (1998), "Verification and Validation in Computational Science and Engineering, " Hermosa Publishers, Albuquerque.

APPENDIX A

The axial velocity, u_b obtained from the stream function satisfying the boundary conditions, ψ_b, is

$$u_b = \frac{1}{H}\left[\frac{\partial f_b(\eta)}{\partial \eta} g_b(\varepsilon) + \left[1 - g_b(\varepsilon)\right]\frac{\partial h_b(\eta)}{\partial \eta}\right] \tag{A.1}$$

where

$$\frac{\partial f_b(\eta)}{\partial \eta} = e^{-\alpha(1-\eta)^2}\left[\pi \sin\left(\tfrac{\pi}{2}\eta\right)\cos\left(\tfrac{\pi}{2}\eta\right) + 2\alpha(1-\eta)\sin^2\left(\tfrac{\pi}{2}\eta\right)\right] \tag{A.2}$$

$$\frac{\partial h_b(\eta)}{\partial \eta} = \pi \sin\left(\tfrac{\pi}{2}\eta\right)\cos\left(\tfrac{\pi}{2}\eta\right) \tag{A.3}$$

The function g_b is given in Eq. (15).

Similarly, the axial velocity obtained from the stream function satisfying the homogenous boundary conditions, ψ_s, is

$$u_s = \frac{1}{H}\left[\frac{\partial f_s(\varepsilon,\eta)}{\partial \eta} g_s(\varepsilon)\right] \tag{A.4}$$

where

$$\frac{\partial f_s(\varepsilon,\eta)}{\partial \eta} = A\left[2\left[\eta - h_s(\varepsilon)\right]\eta(1-\eta)(1-2\eta) + \eta^2(1-\eta)^2\right] \tag{A.5}$$

The function g_s is given in Eq. (19).

The axial velocity field is than obtained as;

$$u = \frac{\partial \psi}{\partial y} = \frac{\partial \psi_b}{\partial y} + \frac{\partial \psi_s}{\partial y} = u_b + u_s \tag{A.6}$$

Finally, the axial velocity expression takes the following form;

$$u = \frac{1}{H}\left[\frac{\partial f_b(\eta)}{\partial \eta} g_b(\varepsilon) + \left[1 - g_b(\varepsilon)\right]\frac{\partial h_b(\eta)}{\partial \eta}\right] + \frac{1}{H}\left[\frac{\partial f_s(\varepsilon,\eta)}{\partial \eta} g_s(\varepsilon)\right] \tag{A.7}$$

Vertical velocity can be obtained in a similar manner;

$$v_b = \frac{1}{L}\left[\frac{\partial g_b(\varepsilon)}{\partial \varepsilon}\left[h_b(\eta) - f_b(\eta)\right]\right] \tag{A.8}$$

$$\frac{\partial g_b(\varepsilon)}{\partial \varepsilon} = -\pi \sin\left(\tfrac{\pi}{2}\varepsilon\right)\cos\left(\tfrac{\pi}{2}\varepsilon\right) \tag{A.9}$$

The functions f_b and h_b appearing in Eq. (A.8) is given in Eq. (13) and Eq. (14) , respectively.

$$v_s = -\frac{1}{L}\left[\frac{\partial f_s(\varepsilon,\eta)}{\partial \varepsilon} g_s(\varepsilon) + \frac{\partial g_s(\varepsilon)}{\partial \varepsilon} f_s(\varepsilon,\eta)\right] \tag{A.10}$$

$$\frac{\partial f_s(\varepsilon,\eta)}{\partial \varepsilon} = -A\left[\frac{\partial h_s(\varepsilon)}{\partial \varepsilon}\eta^2(1-\eta)^2\right] \tag{A.11}$$

$$\frac{\partial h_s(\varepsilon)}{\partial \varepsilon} = -\frac{\pi h_{step}}{2\varepsilon_r}\sin\left(\pi\frac{\varepsilon}{\varepsilon_r}\right) \tag{A.12}$$

$$\frac{\partial g_s(\varepsilon)}{\partial \eta} = B\left[2e^{-\beta\varepsilon^2}\varepsilon(1-\varepsilon)\left[1-2\varepsilon-\beta\varepsilon^2(1-\varepsilon)\right]\right] \tag{A.13}$$

The functions f_s and h_s appearing in Eq. (A.10) is given in Eq. (17) and Eq. (18) , respectively.

The vertical velocity field is than obtained as;

$$v = -\frac{\partial \psi}{\partial x} = -\frac{\partial \psi_b}{\partial x} - \frac{\partial \psi_s}{\partial x} = v_b + v_s \tag{A.14}$$

Finally, the vertical velocity expression takes the following form;

$$v = \frac{1}{L}\left[\frac{\partial g_b(\varepsilon)}{\partial \varepsilon}\left[h_b(\eta) - f_b(\eta)\right]\right] - \frac{1}{L}\left[\frac{\partial f_s(\varepsilon,\eta)}{\partial \varepsilon} g_s(\varepsilon) + \frac{\partial g_s(\varepsilon)}{\partial \varepsilon} f_s(\varepsilon,\eta)\right] \tag{A.15}$$

APPENDIX B

The general mean momentum equation for a turbulent flow can be written in the following way

$$\frac{D}{Dt}u_j = \frac{\partial}{\partial x_i}\left[\upsilon_{eff}\left(\frac{\partial u_i}{\partial x_j}+\frac{\partial u_j}{\partial x_i}\right)\right]-\frac{1}{\rho}\frac{\partial}{\partial x_j}\left(p+\tfrac{2}{3}\rho k\right) \tag{B.1}$$

by incorporating an effective viscosity that is composed of a mean and a deviation from the mean.

$$\upsilon_{eff} = \upsilon_{eff}^{avg} + \upsilon'_{eff} \tag{B.2}$$

X-component of the steady mean momentum equation can be written explicitly as

$$\begin{aligned} u\frac{\partial u}{\partial x}+v\frac{\partial u}{\partial y} &= \frac{\partial}{\partial x}\left[\upsilon_{eff}\left(\frac{\partial u}{\partial x}+\frac{\partial u}{\partial x}\right)\right]+\frac{\partial}{\partial y}\left[\upsilon_{eff}\left(\frac{\partial v}{\partial x}+\frac{\partial u}{\partial y}\right)\right]-\frac{1}{\rho}\frac{\partial}{\partial x}\left(p+\tfrac{2}{3}\rho k\right) \\ &= \upsilon_{eff}\frac{\partial}{\partial x}\left(\frac{\partial u}{\partial x}+\frac{\partial u}{\partial x}\right)+2\frac{\partial u}{\partial x}\frac{\partial \upsilon_{eff}}{\partial x}+\upsilon_{eff}\frac{\partial^2 u}{\partial y^2}+\upsilon_{eff}\frac{\partial}{\partial x}\left(\frac{\partial v}{\partial y}\right)+\left(\frac{\partial v}{\partial x}+\frac{\partial u}{\partial y}\right)\frac{\partial \upsilon_{eff}}{\partial y}-\frac{1}{\rho}\frac{\partial}{\partial x}\left(p+\tfrac{2}{3}\rho k\right) \\ &= \upsilon_{eff}^{avg}\left(\frac{\partial^2 u}{\partial x^2}+\frac{\partial^2 u}{\partial y^2}\right)+S_x \end{aligned} \tag{B.3}$$

where the source term in x-component of the mean momentum equation, S_x is

$$S_x = 2\frac{\partial u}{\partial x}\frac{\partial \upsilon'_{eff}}{\partial x}+\left(\frac{\partial v}{\partial x}+\frac{\partial u}{\partial y}\right)\frac{\partial \upsilon'_{eff}}{\partial y}-\frac{\partial}{\partial x}\left(\tfrac{2}{3}k\right)+\upsilon'_{eff}\nabla^2 u \tag{B.4}$$

Similarly, y-component of the steady mean momentum equation can be written in the form of

$$\begin{aligned} u\frac{\partial v}{\partial x}+v\frac{\partial v}{\partial y} &= \frac{\partial}{\partial x}\left[\upsilon_{eff}\left(\frac{\partial u}{\partial y}+\frac{\partial v}{\partial x}\right)\right]+\frac{\partial}{\partial y}\left[\upsilon_{eff}\left(\frac{\partial v}{\partial y}+\frac{\partial v}{\partial y}\right)\right]-\frac{1}{\rho}\frac{\partial}{\partial y}\left(p+\tfrac{2}{3}\rho k\right) \\ &= \upsilon_{eff}\frac{\partial}{\partial y}\left(\frac{\partial v}{\partial y}+\frac{\partial v}{\partial y}\right)+2\frac{\partial v}{\partial y}\frac{\partial \upsilon_{eff}}{\partial y}+\upsilon_{eff}\frac{\partial}{\partial x}\left(\frac{\partial u}{\partial y}\right)+\upsilon_{eff}\frac{\partial^2 v}{\partial x^2}+\left(\frac{\partial u}{\partial y}+\frac{\partial v}{\partial x}\right)\frac{\partial \upsilon_{eff}}{\partial x}-\frac{1}{\rho}\frac{\partial}{\partial y}\left(p+\tfrac{2}{3}\rho k\right) \\ &= \upsilon_{eff}^{avg}\left(\frac{\partial^2 v}{\partial x^2}+\frac{\partial^2 v}{\partial y^2}\right)+S_y \end{aligned} \tag{B.5}$$

where the source term in y-component of the mean momentum equation, S_y is simply

$$S_y = 2\frac{\partial v}{\partial y}\frac{\partial \upsilon'_{eff}}{\partial y}+\left(\frac{\partial u}{\partial y}+\frac{\partial v}{\partial x}\right)\frac{\partial \upsilon'_{eff}}{\partial y}-\frac{\partial}{\partial y}\left(\tfrac{2}{3}k\right)+\upsilon'_{eff}\nabla^2 v \tag{B.6}$$

Paper No. 32

Discusser's Name: Luis Eça

Question: Is the local proportionality constant of the error estimation changing significantly in the field? Will the procedure handle the possible scatter existing in the data?

Authors' Reply: The constant does change within the field. The scatter does not seem to be as chaotic as that is usually seen in the p-data (i.e. apparent order). The norm, $II\ II_\infty$, applied in the procedure seems to work as a smooth filter. Other filtering approaches can be investigated further.

Discusser's Name: Chris Roy

Question: Your approach is an alternative to Richardson Extrapolation, however you have not shown any comparisons to Richardson Extrapolation. How does your method compare to Richardson Extrapolation?

Authors' Reply: This is a valid point and should be done. However, a similar exercise, an extensive study, within the frame work of 2nd Workshop in CFD uncertainty in Lisbon (Eça and Hoeckstra, 2006) has shown that Richardson Extrapolation has serious problems for the boundary layer problem and especially for the flow past a backward facing step (not the same as the present test case but very similar).

Discusser's Name: Ch. Hirsch

Question: What is the range of validity of your approach on non-uniform grids? I guess that the same type of difficulties as with Richardson Extrapolation should appear.

Authors' Reply: The grid used in the present test cases were already non-uniform grids. Since the present method does not need the grid parameter explicitly, it is directly applicable to non-structured grids. An accurate interpolation scheme from fine grid to course grid is all it is needed.